THE ASTROPHYSICAL JOURNAL, 292:276–290, 1985 May 1

WAVY EDGES SUGGEST MOONLET IN ENCKE'S GAP

JEFFREY N. CUZZI AND JEFFREY D. SCARGLE
Space Science Division, NASA/Ames Research Center, Moffett Field, California
Received 1984 September 4; accepted 1984 November 14

ABSTRACT

Voyager images have revealed radial undulations of the inner and outer edges of the 325 km wide Encke gap in Saturn's A ring. These waves are present at some, but not all, longitudes. Their locations and wavelengths provide strong indirect evidence for the presence of at least one dominant moonlet of about 10 km radius orbiting near the center of the gap. Implications for "shepherding" theory are discussed.

Subject headings: planets: satellites — planets: Saturn

I. INTRODUCTION

The complex structure discovered in the rings of Saturn by the *Voyager* spacecraft has provided a fertile testing ground for a variety of dynamical theories. Especially within the outer (A) ring, gravitational resonances with known satellites external to the rings are of sufficient strength and abundance to account for most of the observed structure (Lissauer and Cuzzi 1982; Holberg, Forrester, and Lissauer 1982; Esposito *et al.* 1984). However, resonances with external satellites are incapable of accounting either for the "record-groove" appearance of the B ring or for the existence of a handful of essentially empty gaps with widths between 50 and 400 km which occur in the A, C, and Cassini Division regions of the rings (Cuzzi *et al.* 1984).

The existence of a population of embedded "moonlets" has been invoked to explain these latter effects. A moonlet exerts a torque on adjacent ring material which results in transfer of momentum to or from the ring (Lin and Papaloizou 1979, Goldreich and Tremaine 1979*a*, *b*, 1980). This "shepherding" process was originally invoked to explain the confinement of the rings of Uranus (Goldreich and Tremaine 1979*a*), but it also predicts the clearing of gaps by moonlets which are embedded within a disk of material (Lissauer, Shu, and Cuzzi 1981; Hénon 1981). Although there are alternate hypotheses for explaining the irregular structure of the opaque rings, such as the viscous instability mechanism (Hameen-Anttila 1978; Lin and Bodenheimer 1981, Ward 1981), no alternative hypothesis exists to explain the existence of several empty gaps at nonresonant locations in the rings. For this reason, it has been a great concern that the only careful and complete search for embedded moonlets as yet conducted—within the 250–400 km wide (eccentric) Huygens gap in the Cassini Division—produced negative results at what was thought to be a threshold capable of disproving the moonlet hypothesis (Smith *et al.* 1982).

However, neither have all candidate gaps been searched, nor is the shepherding theory so well understood that the relationship between gap size and moonlet size is tightly constrained. Therefore, other forms of evidence besides direct detection have been sought. For instance, Saturn's F ring is a clumpy, kinky strand or strands of material, straddled by the 100 km diameter satellites 1980S26 and 1980S27. This configuration is reminiscent of the Goldreich-Tremaine hypothesis for the Uranian case. In addition, Showalter and Burns (1982) have shown that shepherds are capable of producing azimuthal waves and "kinks" in adjacent rings similar to those observed. The physics of this kinking was developed by Julian and Toomre (1966) and described also by Lin and Papaloizou (1979) and Dermott (1981). Encke's gap contains several narrow ringlets qualitatively similar to the F ring; in this paper we report the observation and analysis of edge waves running along the inner and outer edges of the Encke gap. These waves are more easily understood than the kinky ringlets, and strongly support the hypothesis that the Encke gap contains at least one, as yet unseen, embedded moonlet of roughly 10 km radius. In subsequent papers we will present complementary evidence and studies of the kinky ringlets in the Encke gap. We will also systematically explore the edges of other empty gaps. Preliminary, very cursory, investigation has revealed no wavy edges in other gaps such as Huygens or Maxwell.

Section II deals with the observations (*Voyager* images) and techniques for determining wave properties. Section III briefly reviews the relevant physics of local ring-moon interactions. In § IV we compare the observations with theoretical expectations. We also note implications for the distribution of moonlets in the gap and the importance of these results to theories of shepherding.

II. OBSERVATIONAL RESULTS

a) Direct Visual Detection

These edge waves were first noticed on a 35 mm slide of a *Voyager 2* (*V2*) high-resolution image (Flight Data System or FDS number 43993.50) during a stopover in the Albuquerque airport in the autumn of 1981. A horizontally magnified, linear reprojection of this image is presented in Figure 1. A slight residual slope remains on the inner edge which is of no importance to our results. The edge waves are clearly visible on the right-hand (inner) edge of the gap as a smooth, undulating pattern of more or less regular periodicity. The absence of comparable features on the outer edge allows us to immediately rule out instrumental artifacts such as camera distortion or errors in the reprojection process. The waves are also visible in magnified images that are not reprojected.

The radial amplitudes of the edge waves were obtained from direct measurements of pixel coordinates at a particular intensity level along the edge, and subsequent scaling by the known width of the gap (325 km; Marouf and Tyler 1982; cf. also Cuzzi *et al.* 1984). The radial amplitude of the edge displacement determined in this way (one-half of the peak-to-peak variation) is about 2 km. Because the peak-to-peak displacement is comparable to the pixel size, this value is best regarded

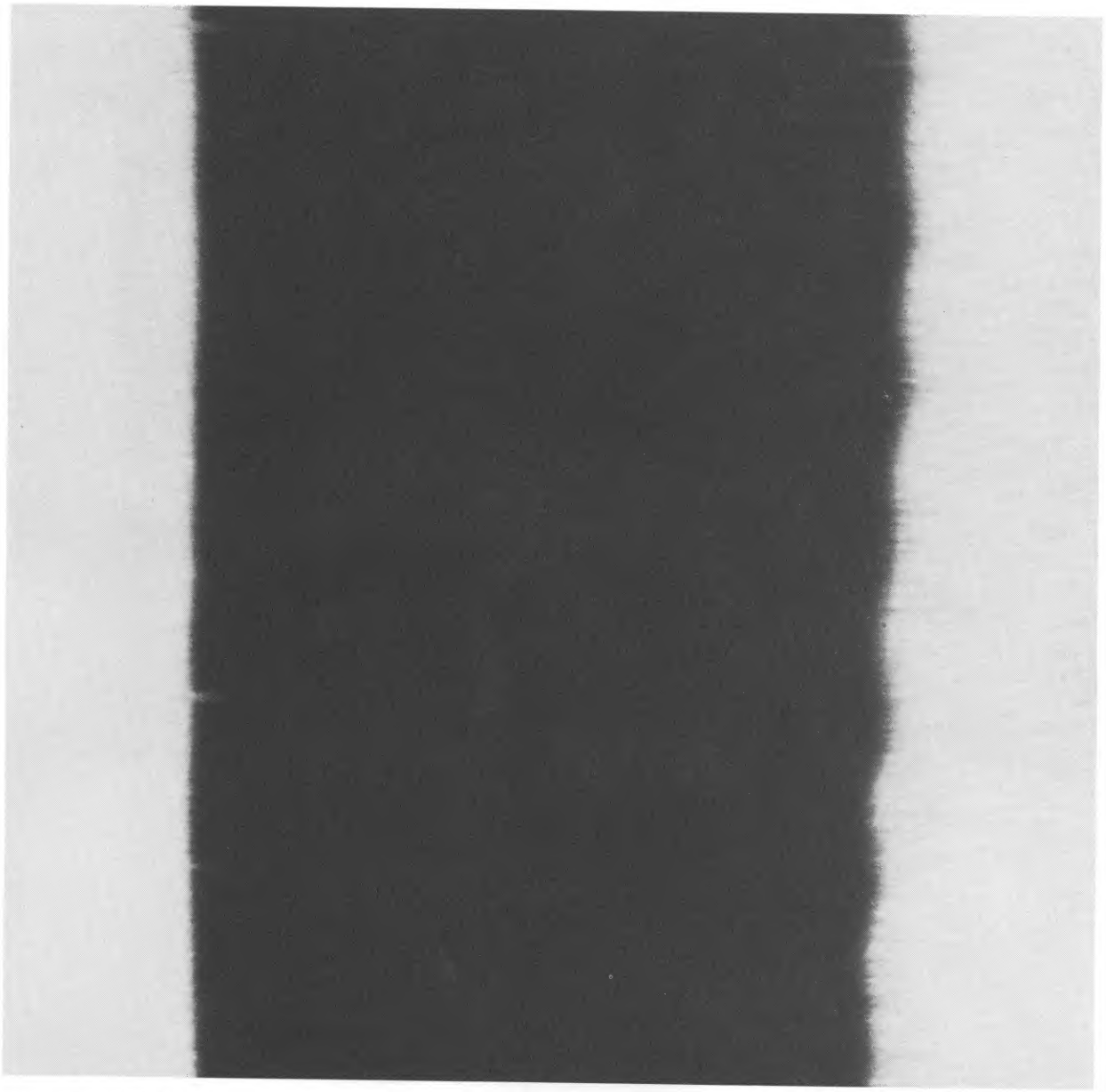

FIG. 1.—*Voyager 2* image FDS 43993.50, linearly reprojected and magnified horizontally by a factor of 10. The dark band is the 325 km wide Encke gap, and a kinky ringlet is seen faintly in the center. Edge waves are seen on the right-hand (inner) edge of the gap. More careful numerical analysis reveals weaker waves on the other edge as well (see Table 1). The radial amplitude of the edge wave is about 2 km.

as an upper limit. Similar investigation of other high-resolution images of the Encke gap revealed other visually detectable edge waves: sometimes only on the inner edge, sometimes only on the outer edge, sometimes on both edges. None of these subsequent edge waves have an amplitude as large as the first one noted. Because most of the waves are of too low an amplitude to be accurately analysed by direct measurements, and because projection effects make it difficult to obtain actual orbital longitudes from the image, we employed a more sophisticated technique which obtains the longitudinal wavelength from spatial frequency analysis of longitudinal scans along the edges of the gap.

b) *Quantitative Analysis: Scans of the Waves*

The basic form of the data used in this analysis is a "scan," obtained by fitting a general conic section to the features on the image, and then reading (using an interpolation and averaging scheme) the digital data along the locus of the conic section and its smoothly interpolated neighbors. We have found that elliptical curves can be made to fit the observed ring features with residuals of less than a pixel. It is also possible to use the Supplementary Experimental Data Record (SEDR), available for each frame from the *Voyager* project, to completely determine the observational geometry in three dimensions. Residual pointing errors in the SEDR tapes may then be removed, or "fixed," using the observed images themselves. In this way, we determine the radial and longitudinal coordinates of each pixel in the frame. Longitudinal scans are then obtained at a series of successively greater displacements into the gap from each edge. At each point in a scan the intensity is averaged over a window 2 or 3 pixels in radial extent. The displacement of the wavy edge in and out of the scan track thus produces an intensity variation proportional to the varying fraction of the window covered by ring material. The longitudinal variation of radial edge displacement thus maps into a longitudinal variation of brightness such as is shown in Figure 2. The horizontal coordinate is a true measure of orbital longitude in the plane of the rings, with all projection effects accounted for.

From scans such as this, wavelengths may be measured directly. However, in the hope of extracting more information in an objective way, we chose to obtain wavelength information from a spatial frequency analysis of the scans. In this way, we not only obtain the wavelength, but also a quantitative measure of how monochromatic the wave is. Put in other terms, we can tell from the structure of the power spectrum whether the edge wave is a single, pure sine wave or a more complex waveform. Representative spectra, including those obtained from the scans in Figure 2, are shown in Figure 3. The spectra in some cases demonstrate the characteristic $(\sin x)/x$ appearance expected for a record of finite length, and the spectral peaks have widths no greater than the resolution of the Fourier transform; therefore such edge waves are monochromatic to within the formal resolution of the method. In Figure 4 we present the average of all spectra shown in Figure 3.

Many images have been analysed in which no edge waves are visible on the images themselves, and occasionally no waves are visible in the scans.

c) *Power Spectrum Analysis of the Scans*

The data were processed in a straightforward way, beginning with a series of standard treatments to remove extraneous effects prior to carrying out the spectral analysis.

Many of the scans had significant trends due to imperfect fitting of the ideal elliptical scan locus, as described above. In the worst cases the intensity rose significantly and then fell,

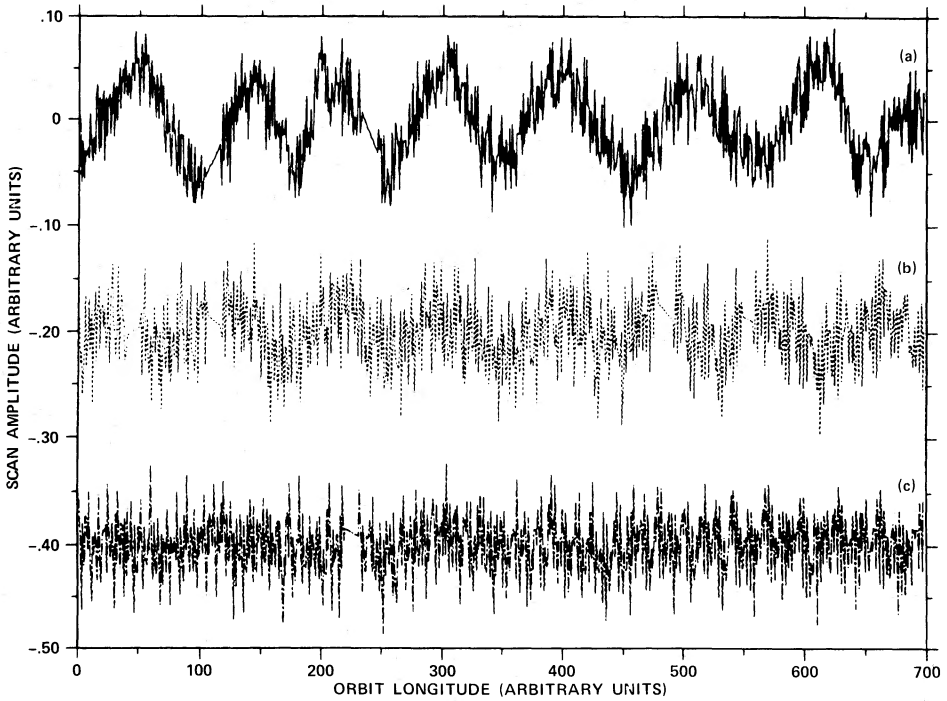

FIG. 2.—Scans representative of (*a*) large amplitude (43990.14 outer edge), (*b*) small amplitude (43999.15 inner edge) but still a definite detection, and (*c*) nondetection (43999.15 outer edge). The detrended and normalized data are plotted as a function of longitude; the longitude range (700 samples) is about 5° in each case.

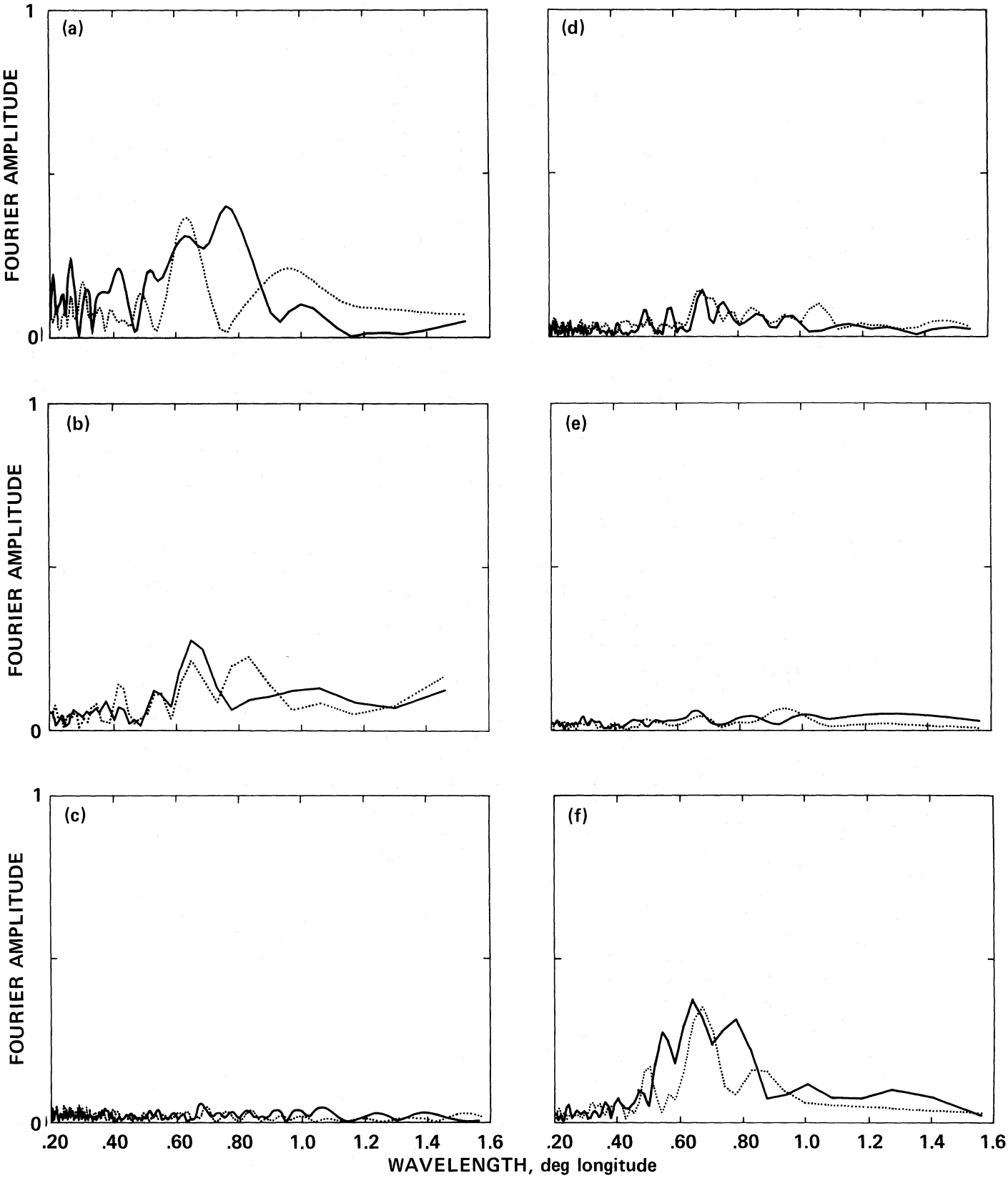

FIG. 3.—Power spectra for the 12 images analyzed. The square root of the power (proportional to the wave amplitude) is plotted against wavelength in degrees of longitude. (*a*) 34934.09, (*b*) 34940.18, (*c*) 43932.27, (*d*) 43968.29, (*e*) 43968.45, (*f*) 43990.14, (*g*) 43993.50, (*h*) 43998.32, (*i*) 43999.03, (*j*) 43999.15, (*k*) 44007.47, (*l*) 44007.59. In each case the solid curve is the outer edge, and the dotted curve the inner edge.

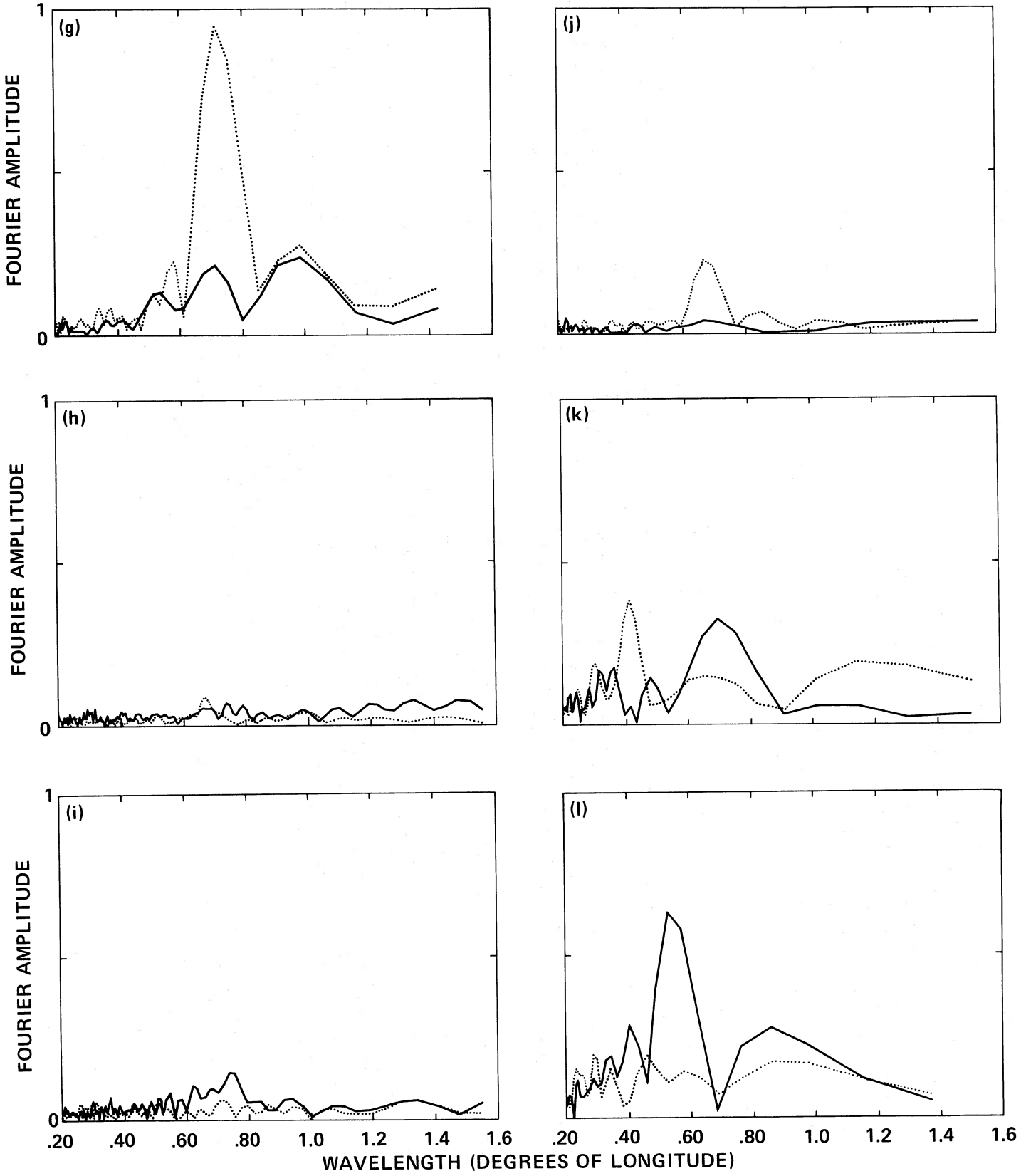

FIG. 3—*Continued*

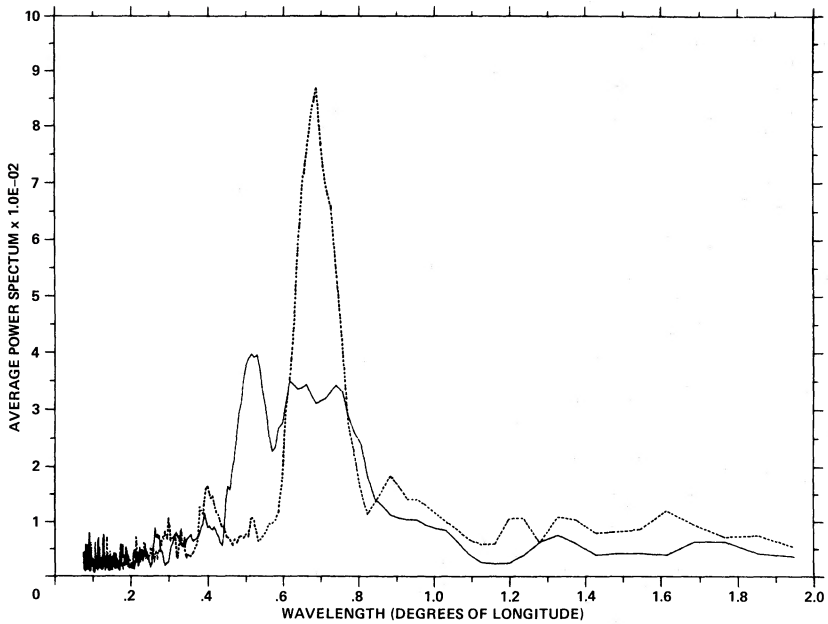

FIG. 4.—Power spectra (not amplitudes) averaged over the 12 pictures reported in Table 1. The solid curve is for the outer edges, the dotted for inner edges. the peak at $\sim 0.^{\circ}5$ on the outer edge is due entirely to FDS 44007.59.

corresponding to the scan track wandering closer to the ring system and then farther from it. The scale of the modulation was much longer than the lengths of the waves, but these trends were removed in order to make the wavelength determination as accurate as possible. Subtraction of a fourth-order least-squares best-fit polynomial removed even strong trends quite cleanly, and this was routinely done to all of the scans. (As a result, the spectra are attenuated to zero at the low-frequency end.)

The next step was to remove any possible systematic variations due to instrumental effects or background, by subtracting out a "background" or comparison scan that lay near the edge in question but entirely within the Encke gap itself. In a few cases ringlets in the gap produced a small signal in even the cleanest such background scan, but this did not appear to affect the spectra significantly.

In addition, the effects of illumination and phase angle were removed by dividing each edge scan by a "normalization" or comparison scan that lay near the edge in question but entirely in the ring system. The data at this point, then, represent the fractional modulation caused by the presence of the wavy edge, corrected for any modulations due to smoothly varying background.

Spectra were originally calculated using window functions, the standard way to diminish the sidelobes of the spectral response function. It was found that this made little difference in the spectra and was not worth the price paid in the form of diminished resolution. Hence all the results and figures given here are for unwindowed spectra.

As can be seen in the sample spectra, many of the scans have a very clean sinusoidal signal. In these cases the determination of the wavelength is straightforward and, in principle, quite precise. Spectra were calculated for a sequence of scans, moving from entirely within the gap to entirely within the ring. The wavelengths and peak powers reported in Table 1 were determined by parabolic interpolation in both wavelength and the scan sequence just described.

The accuracy of this procedure is dependent on the signal-to-noise ratio. In the worst cases, the accuracy is on the order of the fundamental frequency resolution $\omega_0 = 2\pi/L$, where L is the length of the scan in longitude. The relative accuracy in wavelength is thus, at worst, one over the number of wavelengths encompassed by the picture, or typically $\sim 10\%$–15%. In good cases, the peak frequency can be determined with an uncertainty substantially smaller than ω_0. From comparisons of reductions of two halves of the same scan, we judge that the wavelength of a monochromatic signal may be determined to about 1% in the cases of highest signal-to-noise ratio.

The true accuracy, of course, is also affected by errors in the longitude scale of the pictures and geometrical distortion. Errors in the longitude scale, introduced by incomplete correction of the SEDR file, are probably negligible. Comparisons of the longitude scale between "fixed" and "unfixed" SEDR files showed that the corrections are quite small.

However, errors due to camera distortion may be more significant. We used images which were not geometrically corrected in order to avoid degradation of fine-scale edge behavior (on the scale of a pixel). Such images have $\sim 15\%$ compression of scale near corners and are accurate in scale near the center. Most of our scans avoid data within ~ 100 pixels of the edges of the frame. Consequently we expect systematic errors from this source to be less than a few percent.

After reducing the data in this fashion, we noticed the presence of multiple or otherwise complex spectral peaks. In particular, there are four cases of relatively good signal-to-noise ratio where the spectral peak is double or triple. (These are 43968.20 outer, 43990.14 outer, 43993.50 outer, and 34940.18 inner.)

This phenomenon was investigated in some detail by constructing synthetic data consisting of superposed sine waves of various wavelengths and phases. The most straightforward interpretation of a multiple peak—that the disturbance consists of separate signals of different, but close, wavelengths—was rejected for the following reasons. When scans which

TABLE 1—ENCKE GAP EDGE WAVES: LONGITUDE AND WAVELENGTH FOR *Voyager 1* AND *2* IMAGES USED

Image (FDS No.)	Time from Encounter	SHA[a] ($t = 0$)	Edge[b]	Multiplicity[c]	Certainty[d]	Azimuthal Wavelength	Power[e] ($\times 10^2$)	Amplitude[e]	Comments
34934.09.....	−7h.9	208° ± 60	O	D?	1–2	0°.75–0°.62	16.4–9.8	0.093–0.072	noisy but waves visible in scan
	(V-1)	(V-2)	I	S?	1–2	0°.63	13.6	0.074	noisy but waves visible in scan
34940.18.....	−3h.0	181° ± 60	O	S	1	0°.62	8.0	0.043	clean spectral peak
	(V-1)	(V-2)	I	D	2–3	0°.77	5.4	0.035	questionable, but possible, on scan; variation
						0°.61	4.8	0.033	with longitude? Spectrum double or triple
43932.27.....	−2d10h.5	180° ± 5	O	S	3	0°.67	0.36	0.012	poor fits of scans to edge (distortion); low frequencies bad! Complex spectrum but one dominant peak; waves barely visible on scan
			I	S?	4	0°.69	0.20	0.009	questionable; distortion problems
43968.29.....	−1d5h.7	157°	O	M	1–2	0°.68	2.4	0.023	complex spectrum; multiple; phase glitch?
						0°.74	1.2	0.017	two main peaks given; waves visible in scan
			I	S?	1	0°.67–0°.70	2.0	0.020	slightly complex spectrum; possible close double. given as broad single; waves visible in scan
43968.45.....	−1d5h.5	−48°	O	S	1	0°.67	0.54	0.011	pixelation problems in half of scan but visible waves of very different character on first half; only first 165 points reduced
			I	S?	3	0°.98	0.54	0.011	(ditto); waves questionable, spectral peak close to low-frequency noise peak
43990.14.....	−12h.3	250°	O	M	1	0°.73	10.22	0.048	(triple); phase glitch; waves
						0°.62	14.3	0.057	definite
						0°.53	7.9	0.042	
			I	S?	1	0°.80	2.8	0.025	phase glitch; waves definite, but
						0°.64	13.0	0.055	could be single with sidebands
						0.48	3.0	0.026	
43993.50.....	−9h.4	21°	O	M	1–2	0°.90	6.3	0.038	phase glitch? waves weak on scan but good
						0°.67	5.2	0.034	spectrum
						0°.50	1.9	0.021	
			I	S	1	0°.68	94.8	0.147	strong single
43998.32.....	−5h.8	86°	O	...	4–5	...	<0.6	<0.016	nothing visible with certainty
			I	S	2	0°.66	0.82	0.016	weak but probably real
43999.03.....	−5h.2	−36°	O	D?	1	0°.72	2.0	0.02	pixelation problems but part of scan is OK; quoted values based on OK part of scan only; *peak is slightly broad*
			I	...	4	...	<0.5	<0.01	severe pixellation problems; hint of periodicity in scan/spectrum, but hard to trust
43999.15.....	−5h.1	15°.7	O	...	5	...	<0.1	<0.005	...
			I	S	1	0°.65	5.2	0.035	extremely clean; power may be low due to foreshortening in radial direction
44007.47.....	+1h.75	−17°	O	S	1	0°.65	10.7	0.050	noisy; waves look irregular; spectrum has weak multiplicity; evidence for 2d and 3d harmonics
			I	S	2–3	0°.40	14.9	0.058	noisy; ringlet contamination? still possible waves
44007.59.....	+1h.9	−24°[f]	O	S	1	0°.50	40.1	0.090	clean single peak in spectrum
			I	...	3–4	0°.18–0°.54	<4	<0.028	spectrum noisy and cluttered; ringlet contamination? Scans are ambiguous

[a] Add 190°.83 to obtain longitude at $t = 0$ in EME50 system (measured eastward from vernal equinox of 1950.0, along Earth's equator to Ω of ring plane, and thence along ring plane).
[b] O = outer, I = inner.
[c] Multiplicity: S = single, D = double, M = multiple.
[d] Certainty or confidence level: 1 = definite; 2 = probable; 3 = possible; 4 = probably not; 5 = definitely not.
[e] Relative measurements of the strength of the spectral peaks; normalized by the brightness of the background and in the nearby A ring. Typical noise power ($\times 102$) is about 0.1–0.2.
[f] Some possible problems with remaining errors in SEDR file.

produced multiple peaks were divided into two halves and reduced separately, each half typically showed relatively clean single peaks, but at the *same* wavelength. This led to the suspicion that the apparent multiplicity had to do with phase, not wavelength, effects.

Indeed, the scans look to the eye as if there is some kind of jump in the phase. Furthermore, synthetic data consisting of a sine wave of fixed wavelength, but with a sudden jump in phase at one point, produced power spectra which were very similar to the spectra of the actual data. Further confirmation came from fitting sinusoidal models with phase jumps to the data. Figure 5 shows a fit of this kind. The curve is a least-squares fit to the data, but it is not guaranteed to be the global minimum in the residuals. Thus, while the phase jump may not be the only way to interpret these data, we feel that it is plausible. The implications of these observations are discussed further in § IV.

III. EFFECT OF A MOON ON NEARBY RING MATERIAL

The basic physics of our analysis was first developed by Julian and Toomre (1966) in the context of the effect of an orbiting point mass on a surrounding, self-gravitating, differentially rotating disk. To within a numerical coefficient, a simple "impulse" approximation demonstrates the nature of the interaction (Lin and Papaloizou 1979; cf. also Cuzzi *et al.* 1984; Dermott 1984).

Consider a moonlet of mass M in circular orbit at radius $a = a_M$, and separated from a disk of ring material by a distance $s \ll a_M$ (Fig. 6). The moonlet and the nearby ring material have a relative tangential velocity

$$V_{\rm rel} = as d\Omega/da \approx \tfrac{3}{2}\Omega s \ll V_c = \Omega a \,, \qquad (1)$$

where Ω is the local Keplerian orbital frequency and V_c is the orbital velocity. As the ring material, initially in circular orbit, slowly drifts past the moonlet over a typical encounter time $t_e = 2s/V_{\rm rel}$, it experiences a net radial acceleration of order GM/s^2. Thus, at the end of the "encounter," each ring particle has acquired a radial velocity

$$V_\perp = (GM/s^2)t_e \ll V_c \,. \qquad (2)$$

The small radial velocity component $V_\perp$ imparts a small eccentricity to the ring particle orbits, which produces a radial excursion, over one orbit period, of amplitude

$$ae = aV_\perp/V_c = \tfrac{4}{3}(M/M_p)(a/s)^2 a \,,$$

where M_p is the mass of the primary. Qualitatively, the impulse approximation is justified by the fact that the duration of the encounter t_e is much less than the time $P_{\rm syn}$ between encounters ($P_{\rm syn} = 2\pi a/V_{\rm rel} \gg t_e$). However, the encounter is not an impulse on the timescale of an orbit, as $t_e \approx 4a/V_c \approx 2\pi/\Omega$. That is, the effects of rotation are not completely negligible. A more precise calculation, which includes the effect of the rotating frame, yields a numerical coefficient of 2.24 instead of 4/3 in the above equation (Julian and Toomre 1966):

$$ae = 2.24(M/M_p)(a/s)^2 a \,. \qquad (3)$$

Subsequent to the encounter, adjacent particles execute their induced epicyclic motion coherently and freely, without further perturbation by the moonlet until their next mutual encounter one synodic period later. The epicycle is of period $2\pi/\Omega$; in one orbit the ring material moves, relative to the moonlet, an azimuthal distance λ:

$$\lambda = 3\pi s \,. \qquad (4)$$

The epicycle is, of course, repeated every orbital period, and the result is a wavetrain of radial excursions, fixed in the rotat-

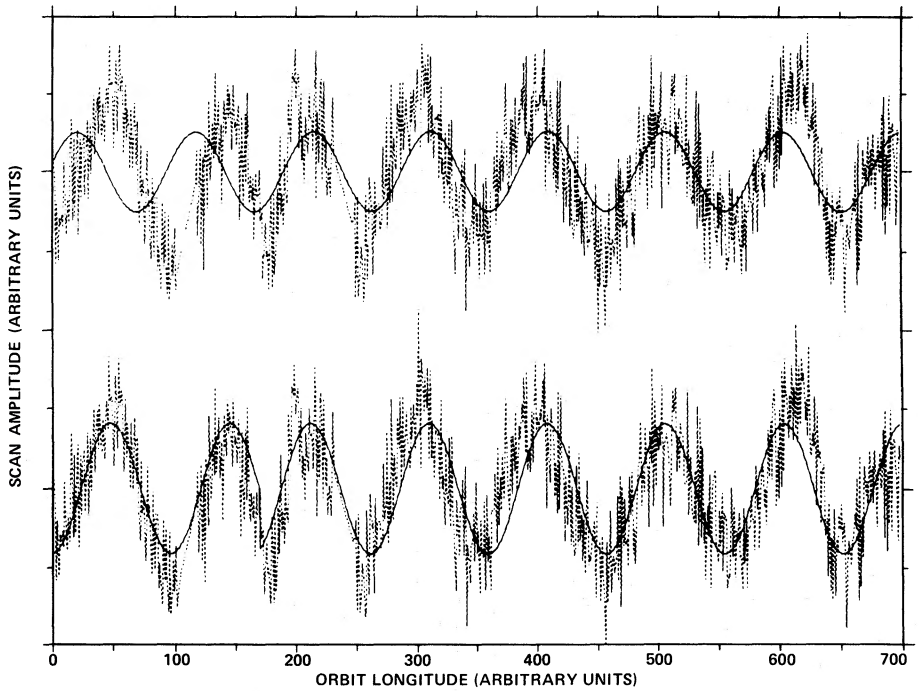

FIG. 5.—Scan of the outer-edge wave on 43990.14 (cf. Fig. 2*a*). The upper trace shows a best-fit sinusoid (*solid line*), while the lower one shows a model consisting of a sinusoid with a fixed amplitude and wavelength, but with a phase jump. The parameters of this model were determined by a nonlinear minimizing routine, and it does not necessarily represent the global minimum. Nevertheless, this result can be taken as strong evidence for the presence of a phase discontinuity (at about 180° on the longitude scale).

ing frame of the moonlet, with azimuthal wavelength $\lambda = 3\pi s$. Each radial extremum represents the apoapsis or periapsis of the orbit of ring particles which encountered the moonlet at successively earlier times. The waves follow the moonlet in the sense of relative motion; that is, trailing if the ring edge is outward of the moonlet and leading if the ring edge is inward of the moonlet. For initially circular orbits, the form of the edge wave is sinusoidal. The radial excursion x of the ring particles from their unperturbed semimajor axis ($a_M \pm s$) may be written in terms of streamline functions as (see Fig. 6):

$$x = ae \sin [(2\pi aL/\lambda) + \phi] = ae \sin (2aL/3s) , \quad (5)$$

where L is longitude in the rotating frame of the moonlet and ϕ is a constant. If the moonlet (or particle) orbits are initially eccentric, the situation is more complex (Showalter and Burns 1982). In this case, both the encounter distance and the relative velocity depend on the relative orbital phase of the encounter. This dependence produces changes in both orbital eccentricity and semimajor axis, and leads to a "kinky" or clumped ringlet appearance much like that seen in the F ring and the Encke gap ringlets. In either case, the azimuthal wavelength, or repetition frequency, depends only on the difference in orbital period, or semimajor axis, between the moonlet and the ring particles. From the standpoint of our spatial frequency analysis, an edge wave caused by a moonlet on an eccentric orbit might show, in addition to the strong periodicity at the "fundamental" wavelength of $3\pi s$, a set of higher harmonics due to deviation of the waveform from a sinusoid. The radial amplitude of the edge wave will also be larger for an eccentric moonlet than for one of equal mass on a circular orbit of the same semimajor axis.

Equations (4) and (5) show how the azimuthal wavelength increases with orbital separation from the perturber. We may draw several interesting predictions from this simple behavior. Because the azimuthal wavelength increases linearly with distance from the perturbing moonlet M, streamlines initially separated by less than $2ae$ eventually intersect. In regions of intersecting streamlines, particle packing density (optical depth) and relative velocities are enhanced over the unperturbed values. We are currently exploring the implications of such variations. One obvious consequence of the enhanced optical depth and relative velocity in regions of streamline crossing is strong collisional damping of the epicycles themselves, and conversion of the forced, coherent motions into dispersion velocities. The details of this damping process are of central importance to the exact manner and rate at which angular momentum and energy are transferred between a moonlet and a nearby ring (cf. Greenberg 1983). These details are not currently well understood. As an example, we may estimate the rate at which the radial streamline excursions, or epicycles, are expected to damp by mutual collisions. Assuming the streamlines to be dynamically independent and to have zero width, the first intersection point occurs at an angle L_i from the moonlet, where

$$dx(L, s)/ds|_{L_i} = 1 = d(ae)/ds \sin (2aL/3s) + aed/ds[\sin (2aL/3s)] . \quad (6)$$

Typical values of ae yield an angular duration of $L_i = 20\lambda$ for the wavetrain. A slightly longer limit of $L_i = 60\lambda$ results from the constraint that waves separated radially by $2ae$ attain a relative phase of π. It seems reasonable to expect collisional damping to be rapid subsequent to streamline intersection within this range of angles. Therefore, we expect to find only $N = L_i/\lambda = 10$–100 waves per train before the edge-wave epicycles are fully damped. However, the observations (see § IV*a*) seem to show a significantly slower damping rate. We do not regard this as a serious problem, but merely as a shortcoming of the assumption that the streamlines are noninteracting. We believe that collective effects due to interactions between streamlines serve to alter trajectories in such a way as to produce a longer damping length, without significantly altering the qualitative physical behavior sketched above. Work is proceeding on this important topic. We return to this point in § V.

IV. DISCUSSION

a) Overall Distribution of the Observed Waves

The locations and wavelengths of all observed edge waves are shown in Figure 7. The angular variable is given in solar hour angle (SHA) at the epoch of *V2* encounter (1981 August 26, 0324 UTC), as described in § II. A simple coordinate transformation gives the correction to longitude in the Earth-Mean-Equator-and-Vernal-Equinox (1950.0) system (see Table 1, n. 1). The reference epoch t_0 was chosen to be the *V2* encounter because most of our good observations are from that encounter. The uncertainty in wave longitude at t_0 depends on the uncertainty in the angular velocity of the wave pattern. In the situation described in § III, the edge waves are fixed in the frame of the moonlet which induces them. That is, their angular velocity is that of the moonlet. The radial separation of the moonlet from the inner and outer edges is determined from the observed wavelength. This fixes the semimajor axis and angular velocity of the moonlet and, therefore, of the associated waves. The formal errors we obtain on edge wavelengths ($< 10\%$) determine the pattern velocity well enough that negligible error results from precession of the *V2* results to t_0. However, the same relative error in wavelength produces a large uncertainty in longitude at t_0 for the *Voyager 1* (*V1*) results, which must be precessed over a far longer time. Consequently, the *V1* results shown in the dashed box in Figure 7, as

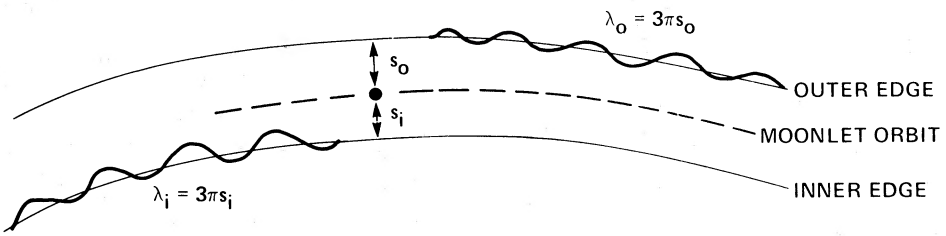

FIG. 6.—Schematic of the effect of a massive orbiting moonlet M on nearby ring material at separation s. The moonlet is at orbital semimajor axis a_M. The schematic is shown in the rotating frame of the moonlet; in this frame, the radial excursions shown are fixed. The radial excursions, or edge waves, lead the moonlet on inner edges and trail it on outer edges. The azimuthal wavelength λ is simply related to s (eq. [4]).

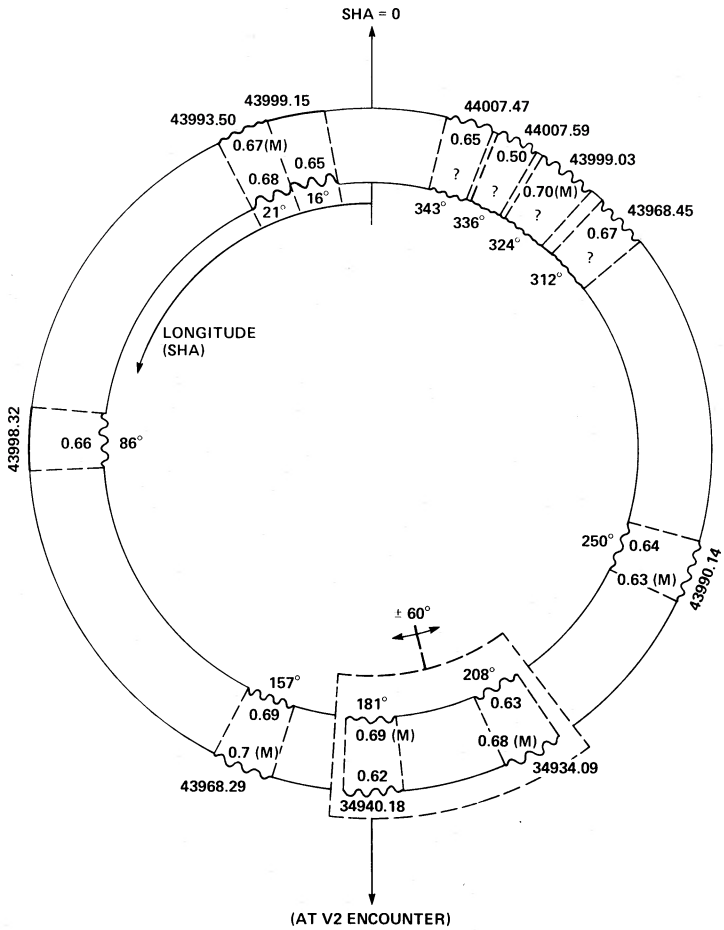

FIG. 7.—The locations of inner and outer edge waves are depicted at the epoch of *Voyager 2* Saturn encounter. In this figure, the origin is at zero solar hour angle (SHA). Questionable waves (class 3–4 in Table 1) are marked (?) on this figure to emphasize the systematic distribution in longitude. The two observations in the dashed box are from *Voyager 1*, and have an azimuthal uncertainty of about ±60°. The waves are labeled by their SHA longitude and by their azimuthal wavelength in degrees. Where the edge spectra are complex, the wavelength is labeled (*M*) for multiple (see § II for discussion).

a unit, are uncertain in longitude by ±60°. In addition, the long time between *V1* encounter and t_0 means that waves of different wavelengths in a given *V1* image, having slightly different pattern speeds, should be precessed at different rates and should not be seen at the same longitude at t_0. The differentials in longitude for the different wavelengths are roughly 20° for the *V1* images. For these reasons we have not attempted to use the *V1* results in any detailed analysis, but include them for completeness and as a consistency check on the primary *V2* results.

Our primary conclusion, that at least one sizable moonlet resides in the Encke gap, is illustrated by the results plotted in Figure 7. Neighboring longitudes at t_0 do, in fact, show consistent behavior, thus weakly supporting the pattern speed chosen for the precession on the basis of the moonlet hypothesis of § III. More important, the pattern sampled at regions between 312° and 21° SHA is consistent in several ways with the effects of a single moonlet, at an intermediate SHA, residing near the center of the gap. This is first seen by the longitudinal distribution of the waves; those on the inner edge lead, and those on the outer edge trail, an intermediate longitude as expected from the sense of differential orbital velocity V_{rel}. Also, to the limits of our method, all the dominant waves in the quadrant near zero SHA are characterized by a monochromatic spectral signature (Fig. 3). With the exception of the anomalous outer edge in FDS 44007.59, the wavelengths observed on a given edge in these neighboring images are all in agreement to within the formal error of ~5%. The observed wavelengths, from equation (4), imply separations for a hypothetical moonlet from the inner and outer edges of 164 km and 160 km respectively. The average separations add up to the width of the gap to (fortuitously) high accuracy. These fundamental properties of the observations support the hypothesis that all the edge waves between 321° and 21° SHA result from a single moonlet orbiting very near the middle of the Encke gap at SHA (t_0) near zero.

b) *Multiple Moonlets and Other Debris*

Consideration of edge structure at other longitudes does not weaken the hypothesis of a moonlet near zero SHA; however, it is important for constraining the number of additional moonlets which may exist in the gap. All longitudes observed between about 150° and 270° exhibit waves of comparable amplitude on both inner and outer edges. Most of these waves are weaker than those near zero SHA, or are obtained from lower resolution images in which systematic effects such as edge pixelation are harder to avoid. Many of the spectra of the edges in this longitude range contain multiple components. Multiple spectral features are also seen on other edges having only weak edge waves (see, e.g., 43993.50 outer edge). The pre-

sence of multiple wavelengths suggests the presence of multiple moonlets near these longitudes. However, as we discussed in § II, the appearance of multiple spectral features does not necessarily imply that the additional perturbers have different semimajor axes. Let us adopt the perspective, following our discussion in § II, that the complex spectra which characterize edges in the region from 150° to 270° SHA "actually" represent a single characteristic wavelength of about 0°.67, and contain occasional phase discontinuities. Such a situation could arise in several different ways.

One simple scenario is that the gap contains multiple moonlets of comparable size which all lie very near the gap center. We may evaluate the likelihood of this sort of configuration by making use of the apparent damping length of the strong, monochromatic waves surrounding zero SHA. It is evident from Figure 7 that the outer edge waves between 312° and 360° SHA must all be due to the same moonlet near zero SHA. If this were not the case, and additional moonlets were to be invoked, their effects would be visible on the inner edge at some or all SHA in this region. Additional evidence (Cuzzi *et al.* 1983) suggests that the responsible moonlet actually lies near an SHA of zero; therefore the damping length D for the waves in the 312°–360° SHA region is probably greater than 60°. If D is no more than about 60°, it is marginally possible to allow moonlets to straddle the image at 250° SHA (43990.14) and generate its inner and outer edge waves separately, without producing detectable inner edge waves at around 312° SHA. It may then be possible for moonlets to exist around 80° and 150° and generate the wave seen on the inner edges of images 43998.32 and 43968.29 without having visible effects on the outer edges of 43993.50 and 43998.32, respectively. No additional constraints may be placed using the images from 180° to 208° SHA, due to uncertainties discussed above and the presence of waves on both edges.

The above scenario, while consistent with the crude theoretical expectations as to the damping length of the waves (10–100 waves) discussed in § III, is somewhat ad hoc. In addition, the long-term dynamical stability of a system of five or more equally massive moonlets with nearly equal semimajor axes is in considerable doubt. A simpler alternative is to postulate that the easily justified moonlet near zero SHA is the only, or at least single dominant, moonlet in the gap. Under these conditions, these "primary" edge waves must be allowed to persist for nearly three-quarters of a synodic period before damping. The production of phase discontinuities and complex spectra at longitudes far from the excitation longitude of the edge wave might still require the presence of additional moonlets in the gap. These additional objects, which only affect strongly damped edge waves, could therefore be considerably less massive than the zero SHA object, and the system could be dynamically stable (e.g. Dermott and Murray 1981). Such a long damping length is difficult to reconcile with the simplified estimates discussed in § III; however, as noted there, important effects are neglected in those estimates of damping length.

In any case, the presence of a single dominant moonlet in the range of SHA between 312° and 20° seems well established. From the wavelengths of the observed edge waves, it seems that this moonlet lies very near the center of the gap. This would be a natural consequence of being in torque balance with ring material on both sides (Lissauer, Shu, and Cuzzi 1981). Using equation (3) and the radial amplitude discussed in § II (2 km), we may estimate the mass of the responsible moonlet. Assuming it to be in circular orbit, we obtain a moonlet mass of about 1.5×10^{-11} Saturn masses (about 10^{19} g), corresponding to a 10 km radius icy object.

Because of sequencing conflicts, no systematic imaging search of the Encke gap was carried out comparable to that which yielded negative results in the Huygens gap of the Cassini division (Smith *et al.* 1982). We have found that no *V2* coverage was obtained of the SHA of our postulated moonlet at sufficiently high resolution to image a 10 km object directly. Work in progress is exploring alternative means of obtaining confirmation of the existence of such an object. We have also searched for possible objects in images which exhibit phase discontinuities in their edge waves. Image 43990.14 has well-defined phase jumps on both inner and outer edges at about the same longitude, and has fairly high resolution (~ 7 km pixel^{-1}). Nothing obvious has been seen in this image at the expected longitude and radial distance; this image is, however, rich in blemishes and also contains a kinky ringlet which extends through the longitudes of interest. If an isolated "icy" moonlet is responsible for the phase jump, its radius is less than a few kilometers. It is not impossible for such an object to cause the observed effect, especially if it is on an eccentric orbit (Showalter and Burns 1982). The orbital eccentricity of such an object could be determined by a balance between occasional increases due to close encounters with the dominant massive moonlet and secular damping due to ring interactions (Goldreich and Tremaine 1980).

One obvious correlation to pursue is that of edge waves with the "kinky" ringlets known to exist in the gap. In our investigations so far, no obvious correspondence has been seen between the longitude or structure of these faint strands of material and the longitude or wavelength of edge waves. It is not likely that a longitudinally extended feature such as a gap ringlet could itself be responsible for the edge wave. In order to produce an "impulse," a perturbing mass is required which has a longitudinal extent much smaller than the observed edge wavelength. At the very least, a significant local density enhancement or clump in the ringlet would be necessary.

It is possible to estimate the size of ringlet particles which could provide a sufficiently massive clump, within the constraints set by other observations. The radial width of the Encke ringlets is about 10 km (Lane *et al.* 1982; Smith *et al.* 1982), and the optical depth τ is about 0.1 (L. Esposito, personal communication, 1983). The optical depth and surface mass density σ are related by:

$$\sigma = n(4\pi\rho/3)r^3 H \approx (n\pi r^2 H)r\rho \sim \tau r\rho \,, \tag{7}$$

where n is particle volume density, ρ is bulk mass density, and H is ring thickness. Consider a clump of longitudinal length l and width w, with mass $lw\sigma$, and recall that l must be much less than the edge-wave wavelength of about 1000 km. Taking $l = 100$ km and $\rho = 1$, we obtain a "particle" radius r of several kilometers. A particle of this size is essentially a moonlet; thus, clumpy ringlets composed of typical meter-sized ring particles will not account for the observations. If localized clumps with an optical depth of several *could* exist stably, particles as small as several hundred meters could provide the necessary mass. However, the increase in brightness of these ringlets with increasing phase angle, as in the case of the F ring, suggests that most of the ringlet particles are much *smaller* than "typical" ring particles. Therefore, the existence of moonlets in the Encke gap of sizes much larger than "typical" ring particles seems unavoidable.

Other evidence also seems to preclude a correlation between

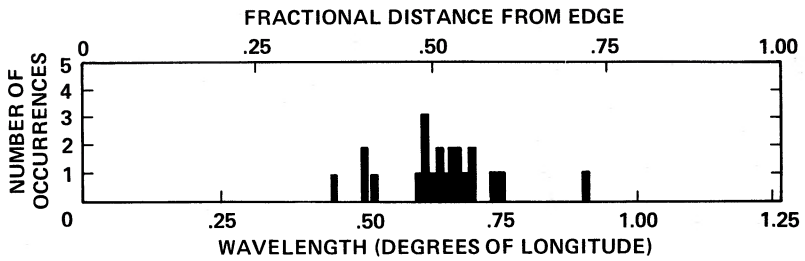

FIG. 8.—Histogram of wavelengths observed for Encke gap edge waves. The horizontal axis is labeled both by wavelength in degrees and by distance from an edge of an object that would produce the corresponding wavelength (see eq. [4]). The shortest and longest possible wavelengths are zero and 1°.3. One kinky ringlet is known to lie near the center of the gap and could be somehow associated with the source of the observed edge waves. However, the other known kinky ringlet lies only 40 km outward of the inner edge; associated material would generate waves at wavelengths of either 0°.1–0°.3 or 1°.2–1°.3. No waves are detected at these wavelengths, leading to a suspicion that the dominant perturbers lie near the center of the gap.

the radial location of the most prominent moonlet(s) and those of the known kinky ringlets. The distribution of observed wavelengths is shown in histogram form in Figure 8, along with implied moonlet-edge separations. Whatever dominant objects are represented in our (rather sparse but longitudinally distributed) sample are clustered near the gap center. This is not true of the kinky ringlets; there is one at only about 40 km separation from the inner edge, and one near the center (Smith *et al.* 1982). Voyager stellar occultation observations show traces of material spread through the outer half of the gap as well (Lane *et al.* 1982). We believe that the possibility of having missed the effects of other large moonlets at other radii is small, because the damping length seems to be at least 60° and perhaps longer; we should be sampling most, if not all, of the edge waves due to major objects. Our spectral analysis technique is, perhaps, insensitive to very long wavelengths (>1°.2) because it is difficult to distinguish such long waves from distortions in the fit to the ring edge (see § II). However, wavelengths shorter than 0°.5, which should be easily detected, are also absent. Specifically, we have not detected any unambiguous short waves in several images which show a conspicuous ringlet near an edge (43990.14, 44007.47, 44007.59). In the case of 44007.59, a complex spectrum is seen for the inner edge which could contain evidence for such short waves, but it is quite noisy and possibly contaminated by the ringlet itself. Based on the existing data, it seems that most, if not all, of the massive objects responsible for clearing the Encke gap reside preferentially near its central region. Clearly, however, a considerable amount of "tinsel" is spread throughout the gap, possibly being resupplied from the more massive, but unseen, embedded moonlets.

c) *Importance to Theories of Shepherding*

Since the discovery of the Uranian rings, several attempts have been made to understand theoretically the properties of the "shepherding" interaction between ring material and a nearby massive object. The interaction, which results in the transfer of angular momentum and energy between the object and the nearby ring material, has been discussed from two seemingly different perspectives: that of an impulse occurring at particle-moonlet conjunction, and that of a series of spiral density waves. Below, we compare and discuss the two perspectives from the standpoint of the observed properties of the Encke gap.

In § III, we have described how ring-particle eccentricities are affected by an impulsive perturbation at closest approach to a moonlet (Lin and Papaloizou 1979). A line of argument from classical dynamics shows how this process allows a net radial transport of ring material to occur (Goldreich, personal communication, 1979; Dermott 1984). In any planar three-body interaction, such as that between the ring particle and a moonlet, a certain combination of the particle's specific (per unit mass) orbital energy E and specific angular momentum J is conserved. This quantity,

$$E_J = E - J\Omega_M \,, \tag{8}$$

is known as Jacobi's constant. Recalling that

$$J^2 = GM_p a(1 - e^2) \,,$$

and

$$E = -GM_p/a = -\tfrac{1}{2}(GM_p/J)^2(1 - e^2) \,, \tag{9}$$

it follows that

$$\Omega_M \Delta J = \Delta E = [(GM_p)^2 \Delta J/J^3 + \tfrac{1}{2}(GM_p/J)^2]\Delta(e^2) \,. \tag{10}$$

This may be rewritten to give the change in specific angular momentum during the encounter ΔJ as

$$\Delta J = -(\Omega a)^2 \Delta(e^2)/(\Omega - \Omega_M) \,. \tag{11}$$

If the particle eccentricity e is always small prior to moonlet encounter, then $\Delta(e^2) = e^2 > 0$, and transport of angular momentum is always outwards; relative to the moonlet, which moves relatively little, inner ring particles fall further inwards, and outer ones move further outwards. The effective specific torque for the interaction is obtained by recalling that the impulse occurs once every synodic period:

$$T = \Delta J/P_{\rm syn} = [(M/M_p)(a^3\Omega/s^2)]^2 \,. \tag{12}$$

Thus we see that a crucial aspect of the shepherding process, as viewed in this perspective, is the damping of the perturbed eccentricities between particle-moonlet encounters. This has also been pointed out by Greenberg (1983). The Encke gap edges offer a valuable illustration of this process in action. The inner edge particles, which move counterclockwise with respect to the moonlet, and the outer edge particles, which move clockwise, show nearly complete damping of their edge waves over a synodic period represented by 360° SHA in Figure 7.

The above torque per unit mass may be rewritten in terms of the torque density in a ring of surface mass density σ as

$$dT/da = (2\sigma/a)\{GM/[s(\Omega - \Omega_M)]\}^2 \tag{13}$$

(Lin and Papaloizou 1979). The total torque on the nearby ring is obtained by integrating equation (13) from s to infinity:

$$T_{\rm total} = (8a\sigma/27s^3)(GM/\Omega)^2 \,. \tag{14}$$

The other perspective from which the shepherding process may be viewed is that of a resonance-wave phenomenon, as developed theoretically by Goldreich and Tremaine (1979*b*, 1980). The moonlet and ring material share a converging series of orbital (Lindblad) resonances with spacings that decrease towards the moonlet. These resonances are at radii where the orbital frequency Ω_R satisfies (in approximate form):

$$(m \pm 1)\Omega_M = (m)\Omega_R \tag{15}$$

for integer m, where

$$m \approx \Omega_M/\Delta\Omega \approx 2a/3s \gg 1 .$$

The relative spacing (Δa) of these resonances is easily shown to be on the order of

$$\Delta a \approx s/m . \tag{16}$$

A characteristic "natural" width may be assigned to each resonance which is related to its location and the mass ratio M/M_p of the responsible object (Goldreich and Tremaine 1982, Dermott 1984). These resonances are capable of exciting spiral density waves such as are seen in several cases of much lower m (e.g., Cuzzi *et al.* 1984). However, because the inter-resonance spacing (Δa) is now less than the natural width of the resonance, the end result is a superposition of waves of varying periodicity. A continuous gravitational torque is envisioned to result in the region of overlapping resonances which is capable of keeping the region clear of material by the usual density-wave transport of angular momentum (Goldreich and Tremaine 1979*a*, Shu 1984). Goldreich and Tremaine (1980, their eq. [18]) have shown that the torque density profile and $T_{\rm total}$ obtained from summing the density wave torque over a series of overlapping resonances is equal to the result obtained from the impulse approximation (eqs. [13] and [14]; Lin and Papaloizou 1979). In some sense, apparently, shepherding has aspects of both sorts of physical behavior much as light has aspects of both wave and particle behavior.

We may compare the total gravitational torque (eq. 14) as determined from either impulse or wave perspective to the viscous torque tending to spread a ring into a clear gap:

$$T_{\rm visc} = 3\pi\nu\sigma\Omega a^2 , \tag{17}$$

where ν is the kinematic viscosity (Lynden-Bell and Pringle 1974). Setting $T_{\rm visc}$ equal to $T_{\rm total}$ gives a relation between the mass M of a moonlet and the width $2s$ of a gap that it is able to keep clear. Substituting $M = 1.5 \times 10^{-11} M_p = 10^{19}$ g (§ IV*b*), and $\nu \approx 200$ cm^2 s^{-1} (Lissauer, Shu, and Cuzzi 1985, Esposito, O'Callahan, and West 1983), we obtain $2s \approx 300$ km, in rough agreement with the 325 km width of the Encke gap. This supports the idea that the Encke gap is cleared by shepherding, and that the zero SHA object accounts for most of the mass required.

Naturally, gaps remain in our understanding as well as in the rings. The torque density profile (eq. [13]) predicted by both impulse and wave approaches was adopted by Lissauer, Shu, and Cuzzi (1981) and Hénon (1981) in estimating the width and structure of gaps in Saturn's rings. A careful search revealed no moonlets of the predicted sizes in the two 200–400 km wide gaps in the Cassini division (Smith *et al.* 1982). A related problem is the detailed profile of the edge of a shepherd-cleared gap such as we now fully believe the Encke gap to be. The edge of the Encke gap is very sharp; it seems to have a radial scale height of less than 200 m (Marouf and Tyler 1982; Lane *et al.* 1982). This is in disagreement with the relatively smooth profiles derived by Lissauer, Shu, and Cuzzi (1981) for an edge in balance between the above viscous torque and the gravitational torque given by equation (13). The explanation of this discrepancy probably lies in the systematics of collisions between particles on perturbed streamlines (Borderies, Goldreich, and Tremaine 1982, 1984), although the details are far from understood. Also, certain of the density-wave aspects of the phenomenon might help us to better understand the observed behavior of the Encke gap edges and shepherded rings in general.

Finally, we note that these observations and insights as to the properties of shepherded rings may provide us with an explanation for the behavior of certain of the Uranian rings. Ongoing stellar occultation observations have refined the orbit models of these rings to within observational residuals of a few hundred meters. Yet several of the observed Uranian ring central radii and/or widths exhibit a scatter of up to several km from the best fitting ellipse and/or smooth, linear relation of ring width to distance from the planet (French and Elliot 1984; Elliot and Nicholson 1984). These discrepancies may be due to wavy edges induced on these rings by their shepherds. If *Voyager* images are able to detect edge waves and/or kinks in the Uranian rings, an important unifying characteristic of planetary ring-moon systems will be at hand.

V. CONCLUSIONS

In this paper we have presented evidence which supports the presence of a 10 km radius moonlet orbiting within the Encke gap in Saturn's rings. The evidence consists of wavy radial excursions in the orbits of ring material along the inner and outer edges of the gap. The locations and wavelengths of the observed waves suggest that a single moonlet dominates the gap, but some smaller objects are also probably present with sizes still far larger than typical 1–100 cm sized ring particles. We believe that the morphology of these wavy edges and the relationship of edge waves to gravitational torque illustrate clearly for the first time the basic working of the shepherding process; however, many open questions remain as to the details of the observed structure and the mechanism responsible.

We would like to thank our colleagues on the *Voyager* imaging team, especially A. Bunker, A. Collins, B. Smith, and L. Soderblom, for their support in obtaining the images analysed here. We also thank J. Holberg and E. Marouf for help with the geometry of the observations; M. Legg, K. Bilski, and K. Fischer for their careful data analysis; and M. Haas for patient assistance with various computational matters. We have greatly profited from helpful conversations with many other colleagues, especially F. Shu, M. Showalter, N. Borderies, J. Lissauer, and P. Goldreich.

REFERENCES

Borderies, N., Goldreich, P., and Tremaine, S. 1982, *Nature*, **299**, 209.
———. 1984, in *Planetary Rings*, ed. A. Brahic and R. Greenberg (Tucson: University of Arizona Press), p. 713.
Cuzzi, J. N., Lissauer, J. J., Esposito, L. W., Holberg, J. B., Marouf, E. A., Tyler, G. L., and Boischot, A. 1984, in *Planetary Rings*, ed. R. Greenberg and A. Brahic (Tucson: University of Arizona Press), p. 73.
Cuzzi, J. N., Scargle, J. D., Showalter, M. R., and Esposito, L. W. 1983, *Bull. AAS*, **15**, 813.
Dermott, S. F. 1981, *Nature*, **290**, 454.
———. 1984, in *Planetary Rings*, ed. R. Greenberg and A. Brahic (Tucson: University of Arizona Press), p. 589.
Dermott, S. F., and Murray, C. D. 1981, *Icarus*, **48**, 12.

Elliot, J. L., and Nicholson, P. D. 1984, in *Planetary Rings*, ed. R. Greenberg and A. Brahic (Tucson: University of Arizona Press), p. 25.
Esposito, L. W., Cuzzi, J. N., Evans, D. R., Holberg, J. H., Marouf, E. A., Tyler, G. L., and Porco, C. C. 1984, in *Saturn*, ed. T. Gehrels (Tucson: University of Arizona Press), p. 463.
Esposito, L., O'Callahan, M., and West, R. A. 1983, *Icarus*, **56**, 439.
French, R. G., and Elliot, J. L. 1984, *Bull. AAS*, **16**, 677.
Goldreich, P., and Tremaine, S. 1979*a*, *Ap. J.*, **233**, 857.
———. 1979*b*, *Nature*, **277**, 97.
———. 1980, *Ap. J.*, **241**, 425.
———. 1982, *Ann. Rev. Astr. Ap.*, **20**, 249.
Greenberg, R. 1983, *Icarus*, **53**, 207.
Hameen-Anttila, K. A. 1978, *Ap. Space Sci.*, **58**, 477.
Hénon, M. 1981, *Nature*, **293**, 33.
Holberg, J. B., Forrester, W., and Lissauer, J. J. 1982, *Nature*, **297**, 115.
Julian, W., and Toomre, A. 1966, *Ap. J.*, **146**, 810.
Lane, A. L., *et al.* 1982, *Science*, **215**, 537.
Lin, D. N. C., and Bodenheimer, P. 1981, *Ap. J. (Letters)*, **248**, L83.
Lin, D. N. C., and Papaloizou, J. 1979, *M.N.R.A.S.*, **186**, 799.
Lissauer, J. J., and Cuzzi, J. N. 1982, *A.J.*, **87**, 1051.
Lissauer, J. J., Shu, F. H., and Cuzzi, J. N. 1981, *Nature*, **292**, 707.
———. 1985, in *IAU Colloquium 75, Planetary Rings*, ed. A. Brahic, in press.
Lynden-Bell, D., and Pringle, J. E. 1974, *M.N.R.A.S.*, **168**, 603.
Marouf, E. A., and Tyler, G. L. 1982, *Science*, **217**, 243.
Showalter, M. R., and Burns, J. A. 1982, *Icarus*, **52**, 526.
Shu, F. H. 1984, in *Planetary Rings*, ed. R. Greenberg and A. Brahic (Tucson: University of Arizona Press), p. 513.
Smith, B. A., *et al.* 1982, *Science*, **215**, 504.
Ward, W. R. 1981, *Geophys. Res. Letters*, **8**, 641.

JEFFREY N. CUZZI and JEFFREY D. SCARGLE: Space Science Division, 245-3, Ames Research Center, NASA, Moffett Field, CA 94035